A far UV study of interstellar gas towards HD 34078: High excitation H2 and small scale structure

F.Le Petit, E. Rollinde, E. Roueff, G.Pineau Des Forêts, B.-G. Andersson, C. Gry, P. Boissé, P. Felenbok

A&A 429, 509–523 (2005)
DOI: 10.1051/0004-6361:20047135

Astronomy & Astrophysics

A far UV study of interstellar gas towards HD 34078: High excitation H_2 and small scale structure⋆

P. Boissé[1,2], F. Le Petit[3,4], E. Rollinde[1,5], E. Roueff[3], G. Pineau des Forêts[6,3], B.-G. Andersson[7], C. Gry[8,9], and P. Felenbok[10]

[1] Institut d'Astrophysique de Paris, 75014 Paris, France
[2] LERMA/ENS, France
[3] LUTH, Observatoire de Paris-Meudon, 92195 Meudon Cedex, France
[4] Onsala Space Observatory, 439 92 Onsala, Sweden
[5] Institute of Astronomy, Cambridge, UK
[6] IAS, Université d'Orsay, 91405 Orsay Cedex, France
[7] Johns Hopkins University, Baltimore, USA
[8] ESA, Vilspa, Spain
[9] Laboratoire d'Astrophysique de Marseille, 13376 Marseille, France
[10] LESIA, Observatoire de Paris-Meudon, 92195 Meudon Cedex, France

Received 24 January 2004 / Accepted 12 July 2004

Abstract. To investigate the presence of small scale structure in the spatial distribution of H_2 molecules we have undertaken repeated FUSE UV observations of the runaway O9.5V star, HD 34078. In this paper we present five spectra obtained between January 2000 and October 2002. These observations reveal an unexpectedly large amount of highly excited H_2. Column densities for H_2 levels from ($v = 0$, $J = 0$) up to ($v = 0$, $J = 11$) and for several $v = 1$ and $v = 2$ levels are determined.
These results are interpreted in the frame of a model involving essentially two components: i) a foreground cloud (unaffected by HD 34078) responsible for the H_2 ($J = 0, 1$), CI, CH, CH^+ and CO absorptions; ii) a dense layer of gas ($n \simeq 10^4$ cm^{-3}) close to the O star and strongly illuminated by its UV flux which accounts for the presence of highly excited H_2. Our model successfully reproduces the H_2 excitation, the CI fine-structure level populations as well as the CH, CH^+ and CO column densities.
We also examine the time variability of H_2 absorption lines tracing each of these two components. From the stability of the $J = 0$, 1 and 2 damped H_2 profiles we infer a 3σ upper limit on column density variations $\Delta N(H_2)/N(H_2)$ of 5% over scales ranging from 5 to 50 AU. This result clearly rules out any pronounced ubiquitous small scale *density* structure of the kind apparently seen in HI. The lines from highly excited gas are also quite stable (equivalent to $\Delta N/N \leq 30\%$) indicating i) that the ambient gas through which HD 34078 is moving is relatively uniform and ii) that the gas flow along the shocked layer is not subject to marked instabilities.

Key words. stars: individual: HD 34078 – ISM: structure – ISM: molecules – ISM: clouds

1. Introduction

Studies of the molecular phase of the interstellar medium are severely hampered by the fact that the most abundant species, H_2, cannot be observed from the ground. "Tracers", like CH, CO and its isotopomers are often used as surrogates; however, because of selective photodissociation near the illuminated boundaries of clouds, depletion onto grains in their depths or, simply, time evolution under the coupled effect of internal dynamics and chemistry, no tight relation is expected between the *local* abundance of H_2 and those of minor species. In other words, the widely used notion of "standard" ratios can hardly be justified, even if, when integrated along the line of sight, the amounts of various species appear relatively well correlated.

The above limitation is especially severe when we deal with small scale structure studies. Within translucent molecular clouds, H_2CO, OH and HCO^+ molecules have been found to display AU-scale structure (Moore & Marscher 1995; Liszt & Lucas 2000). In contrast, the distribution of dust grains is quite smooth at small scales, both in translucent and dense material (Thoraval et al. 1996, 1997, 1999; Lada et al. 1999; Alves et al. 2001). If H_2 were to display marked AU-scale structure, as minor molecular species apparently do, then the smooth behavior of dust grains could be understood as a result of their large inertia (Thoraval et al. 1999). However, it could also be that the H_2 distribution is smooth at small scales with no or little density structure (like dust grains) and that "chemical"

⋆ Based on observations performed by the FUSE mission and at the CFHT telescope.

inhomogeneities are present. Clearly, direct investigations of the distribution of H_2 itself are needed to clarify the above issues and determine whether the structure seen for minor species is due to fluctuations of their local abundance or rather reflects real *density* structure.

We have thus taken advantage of the unique opportunity offered by the successful launch of FUSE and proposed a GI program which aims at probing the distribution of H_2 over spatial scales ranging from about 1 to 100 AU. A bright O9.5V star, HD 34078 (AE Aur) has been selected for repeated observations and, thanks to its large proper motion (Moffat et al. 1998), information on the structure of the foreground medium can be obtained within a relatively small time interval. Indeed, at a distance of 530 pc the implied transverse velocity is 103 km s^{-1} or 22 AU/yr. Its color excess, $E(B-V) = 0.52$, is such that a significant fraction of the foreground gas should be in molecular form. It is also of interest that the velocity structure of the molecular gas along this line of sight is quite simple, with only one major component that has $b \approx 3$ km s^{-1} (Allen 1994; Rollinde et al. 2003). In the following, we shall adopt a distance of 380 pc for this molecular material (Brown et al. 1995), implying a drift of the line of sight through the cloud at a velocity of 17 AU/yr. Note finally that HD 34078 has been the subject of several detailed studies in the past decade that have brought results on a number of molecular species including CH, CH^+, CN, C_2 (Federman et al. 1994; Herbig 1999). The latter can be helpful for modelling and the past measurements provides information on structure over larger scales by comparison with present-day observations. In particular, a series of observations of the blue CH and CH^+ lines has been performed since 1999 in parallel with this FUSE program (Rollinde et al. 2003). Results indicate a long-term increase of N(CH) over the past 10 years while $N(CH^+)$ remained stable or decreased. Correlated short-term ($\simeq$1 yr) CH and CH^+ fluctuations might also be present.

The first FUSE spectrum obtained revealed large amounts of high excitation H_2. This is an unexpected finding in comparison with observations of most other lines of sight (see however Meyer et al. 2001 for HD 37903 and Federman et al. 1995). As HD 34078 is a high velocity star, it is likely to be far away from its parent cloud and should hence not be associated with molecular material. This result has important implications for the identification of physical processes responsible for the unusual excitation but could be a difficulty for our structure study. Indeed, the presence of highly excited H_2 raises the possibility of a significant contribution to the observed absorptions from gas associated with the star itself, which could be subject to variability of a different nature than the one due to structure in the foreground gas. The first objective of this paper therefore becomes to establish a reasonable scenario for the origin of the observed absorption, based on detailed modelling of the HD 34078 FUSE spectra. Secondly, we present a study of the variability of the H_2 lines based on five spectra spanning a period of 2.7 years.

In Sect. 2, we describe the FUSE observations and data analysis. Complementary OH observations performed at the CFHT are presented in Sect. 3. Results on the gas properties are discussed in Sect. 4 with their implications, as inferred from modelling of the physical conditions in the absorbing material. We next investigate H_2 line variations (Sect. 5). Preliminary analyses of the first three FUSE spectra have been presented by Le Petit et al. (2000, 2001) and Boissé et al. (2001).

2. The FUSE data

2.1. Observations and data reduction

The first FUSE spectrum was obtained on 2000 January 23; it consisted of eleven exposures with a total integration time of 7145 s. Four other spectra were acquired in comparable conditions on 2000 October 30, 2001 February 16, 2001 October 15 and 2002 October 10 (cycle 1 and 2 programs). The data were taken in histogram (HIST) mode. In this paper we rely mostly on the first spectrum for the study of the intervening gas properties, but occasionally we use the other four, either to secure detections of faint lines or to improve the accuracy of column density estimates. The search for variable H_2 absorption has been performed mainly by comparing the 1st and 5th spectra, because i) they turn out to be of very similar "quality" (resolution and *S/N*); ii) they sample the largest time interval (i.e. largest spatial scales, over which changes might be easier to detect in the event of a regular variation). For absorption lines that are suspected to vary in time, measurements are performed on the first spectrum.

Standard processing using the FUSE pipeline software was applied to perform the wavelength and flux calibration (for details on the FUSE mission, see Moos et al. 2000 and Sahnow et al. 2000). The analysis presented here is based mostly on the LiF1A and LiF1B spectra, which display the highest *S/N* ratio.

The data were reduced in a standard way using MIDAS, the ESO data reduction software package. Comparison of individual exposures occasionally revealed variations in absorption line positions from one exposure to another. Nevertheless, these remain quite small and the average spectrum obtained after applying the appropriate shifts does not differ significantly from the raw average. The original pixel corresponds to 0.005 Å but, given the resolution provided by FUSE (about 20 km s^{-1}) the spectra were binned to 0.015 Å. In the co-added spectrum, the *S/N* ratio reaches 30 per 15 mÅ pixel which translates into a 3σ limit on the equivalent width (W) as low as 4 mÅ.

2.2. Line identification and column density determinations

Line identification has been performed using the list provided by Morton (2000) for atoms and ions. For H_2 transitions we use the data from Abgrall et al. (1993a,b). Originally, only lines from $v = 0$ with $J = 0, 1, ..., 9$ levels were considered. As it turned out that lines from higher excited levels were present in our spectra, the table was complemented by adding transitions from $v = 0$, $J = 10, 11, 12, 13$; $v = 1$, $J = 0, ..., 9$ and $v = 2, 3, 4$, $J = 0, 1, 2$.

To perform the line identification, we proceed in two steps. We first measure the position of all prominent absorption lines in the spectrum and assign one (or several) transitions to each of them. Next, we search in a systematic way for all strong transitions expected in our range and examine whether all

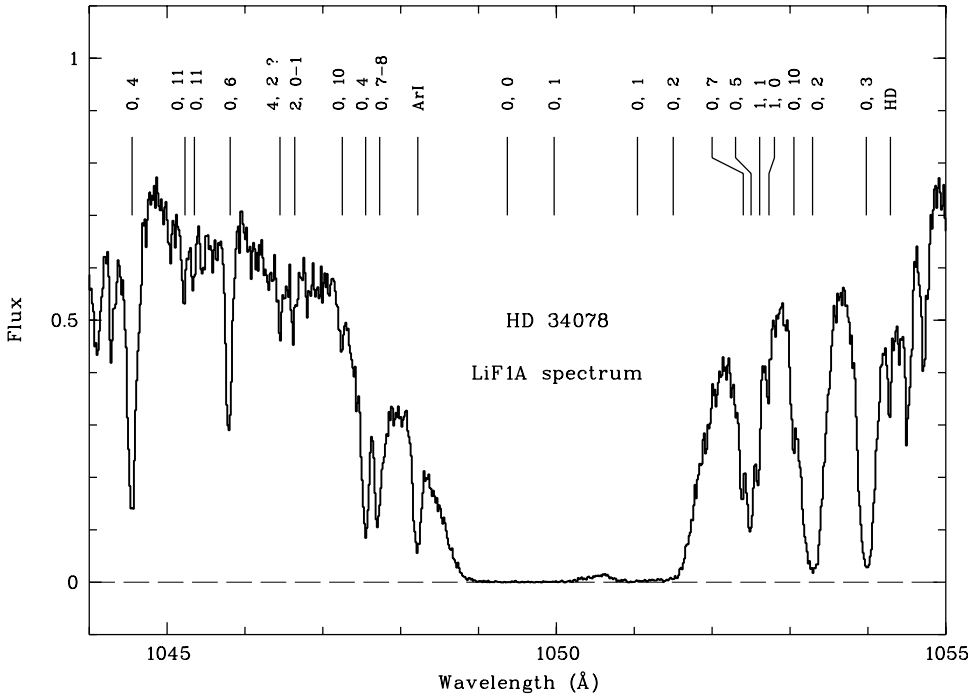

Fig. 1. Portion of the January 2000 LiF1A spectrum in units of 10^{-11} erg s^{-1} cm^{-2} Å^{-1} near strong H_2 (J = 0, 1, 2) lines from the (4–0) Lyman band. v and J values for the lower level of each H_2 transition involved are given. The features indicated illustrate the variety of excited H_2 levels from which absortion is detected. The identification of the feature noted "4, 2 ?" is uncertain (see text in Sect. 2.3).

detections/non-detections and W values for any given species (or particular level of a species) are mutually consistent. This step is a crucial one here since, given the high number density of absorption lines in the spectrum, blends are numerous and the continuum level is often ill-defined (we estimate that in the 1040–1060 Å interval for instance, the fraction of the spectrum free of absorption is no larger than 25%; this fraction becomes close to zero above 1100 Å). As a result of this crowding, some lines may appear either too strong in the event of an unresolved blend or too faint if adjacent absorption leads to an underestimate of the continuum level. When an unresolved blend or ill-defined continuum is suspected, the corresponding feature is not used for column density determination. A portion of the LiF1A spectrum is shown in Fig. 1 where several high excitation H_2 lines are identified.

Except for damped H_2 lines, most features are not resolved (recall that $b \simeq 3$ km s^{-1} for molecular gas towards HD 34078). Further, the line spread function is not accurately known and may vary across the spectrum; we then often rely on curve of growth analysis to derive column densities. However, line fitting is required to deal with partially resolved blends and damped H_2 lines. To this purpose, we use the routine OWENS developed by Martin Lemoine and the LYMAN context in MIDAS. In a first step, the spectrum is shifted to zero velocity using narrow features located blueward and redward of the absorption considered. When fitting damped H_2 profiles, the continuum is interpolated using low order polynomials. Good fits are easily obtained as shown in Fig. 2. For low J values, several H_2 systems are available that can be used to get independent column density estimates (hereafter N), which helps to further reduce the uncertainties.

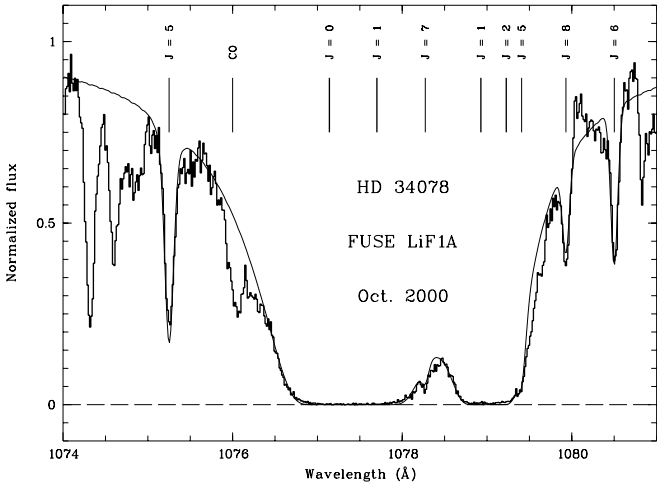

Fig. 2. Portion of the October 2000 LiF1A FUSE spectrum comprising the strong H_2 (2–0) Lyman band around 1078 Å (thick line). The fit obtained when including the nine H_2 lines indicated (v, J values for the lower level are given) is superimposed (thin line); thick tick marks indicate the four strong damped H_2 lines from J = 0, 1, 2. The absorption near 1076 Å is from CO.

Damped lines from low energy H_2 levels provide a measurement of N which is independent of the velocity distribution of the gas; for a b parameter of about 3 km s^{-1} (as measured for CH), we find that this is true up to $J = 3$. The situation is less comfortable for lines of intermediate optical depth. Indeed, difficulties in defining the continuum or due to blends are such that for most H_2 levels we cannot build a curve of growth appropriate for deriving both the b parameter and N. We have to assume some a priori b value. To investigate the possibility of

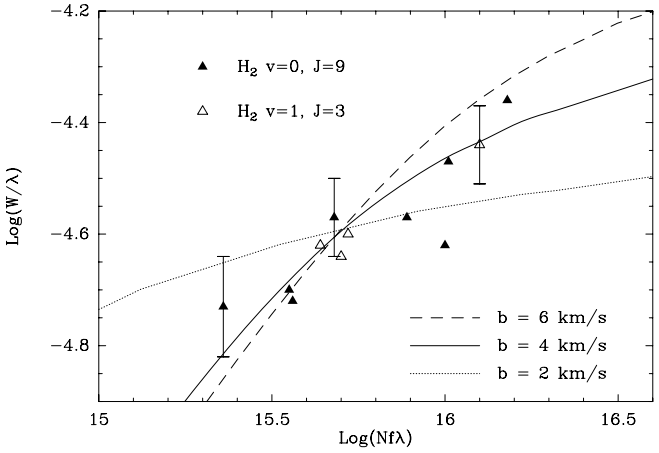

Fig. 3. Curve of growth for H_2 transitions from the $v = 0$, $J = 9$ and the $v = 1$, $J = 3$ levels (filled and empty triangles respectively). The horizontal scale is appropriate for $b = 4$ km s^{-1}; the slopes of the curve of growth corresponding to $b = 2$ and $b = 6$ km s^{-1} are indicated (dotted and dashed line, respectively). A few representative 1σ error bars are given.

a variation in b with excitation energy, we searched for highly excited levels ($J > 5$) for which our data can be used to constrain the b value. Thus, for the ($v = 0$, $J = 9$) level, we get reliable measurements for 8 transitions with $\log(\lambda f)$ values ranging from 0.75 to 1.57 (cf. Fig. 3). We also include three measurements from the ($v = 1$, $J = 3$) level which is close to the previous one in the energy scale. As can be seen in Fig. 3, both levels give consistent constraints on the curve of growth. From these, we estimate that a b value of about 4 km s^{-1} is consistent with the data and find that values below 2 and above 6 km s^{-1} are excluded. We therefore find no evidence that the velocity distribution of the high excitation H_2 differs from that of CH, which presumably reflects that of the bulk of H_2. Note that Meyer et al. (2001) reach a similar conclusion for highly excited H_2 detected in front of HD 37903 (the b value being 1.8 km s^{-1} in this case). In practice we shall adopt $b = 4$ km s^{-1} for $J > 3$.

Optically thin H_2 lines can also be of interest for deriving N without any assumption on the velocity distribution, and for providing reliable constraints on the upper end of the excitation diagram. For $b = 4$ km s^{-1} we estimate that a line around 1000 Å and with an equivalent width of less than 8 mÅ can be considered to be optically thin (the N values derived either from the exact $N(W)$ relation or the linear approximation differ by less than 10%). This is significantly above our detection limit and we do detect H_2 features of this type from the $v = 0$, $J = 10$ and $J = 11$ or some $v = 1$ levels. Non-detections in regions with good *S/N* can also be used to derive upper bounds on N (e.g. for H_2 $v = 0$, $J = 12$ and 13).

Table 2 summarizes the results obained for $N(H_2, v, J)$ and gives the best values together with 3σ lower and upper bounds. The latter have been estimated in a conservative way. When different lines from the same level provide discordant results for N, we adopt the best compromise by weighting various estimates according to the presence of suspected blends and quality of the data. The number of lines effectively used in the determination of N is given in Table 2 as M_1. For lines which are neither in the damped or optically thin regime, an uncertainty on b of ± 1 km s^{-1} was considered.

2.3. Comments on specific H_2 levels or species

In the following, we give some details concerning the column density determination for:

• H_2 $J = 0$, 1, 2: for the absorption from these levels, the continuum level and shape across the broad profiles is difficult to define. To get an estimate of the unabsorbed spectrum, we have artificially removed all narrow features other than those from H_2 $J = 0$, 1, 2. We then simultaneously fit the latter using OWENS; a polynomial form of order 3 has been adopted for the continuum. Fortunately, $N(J = 0, 1, 2)$ is well constrained by the profile near the bottom of the line and weakly depends on the exact shape of the adopted continuum.

• H_2 $J = 3$, 4, ..., 9: for these levels, the number of lines available ranges from 1 ($J = 7$) to 10 ($J = 9$).

• H_2 $v = 0$, $J = 11$: this is the highest $v = 0$ transition detected. Two features are seen at 1045.22 and 1045.35 Å with $W = 10 \pm 2$ mÅ and $W = 7 \pm 2$ mÅ.

• H_2 $v = 0$, $J = 12$ and 13: lines at 1057.62 and 1072.73 Å from $J = 12$ are expected in good "windows"; from their absence we get the upper limit $N < 2.4\times10^{13}$ cm^{-2}. The strongest transition in our range from $J = 13$ is expected at 1040.70 Å ($f = 0.0237$) and is marginally present (2σ detection). We infer the upper limit: $N < 2.7 \times 10^{13}$ cm^{-2}.

• H_2 $v = 1$: several features are seen from each of the $J = 0$ to 5 levels. Therefore, their identification is secure. In contrast, no feature from the ($v = 1$, $J = 6$, 7, 8) levels could be measured due to blending with strong absorptions.

• H_2 $v = 2$, 3, 4: a blend of the 1046.62 and 1046.66 Å lines (from $v = 2$, $J = 1$ and 0 respectively) is marginally detected with $W = 12$ mÅ in the 1st, 4th and 5th spectra, which have the best resolution and *S/N* in this region. Unfortunately, we do not find other lines suitable for the determination of $N(v = 2, J = 0)$ and $N(v = 2, J = 1)$ separately.

Regarding $v = 3$ levels, several lines are suspected to be present but have a low significance level. For instance, a line from ($v = 3$, $J = 1$) is seen in the 1st and 4th spectra at 1116.405 Å with $W = 3 \pm 1.5$ mÅ. The corresponding column density is $N = 6 \times 10^{12}$ cm^{-2}. However, most of these lines are expected at $\lambda > 1100$ Å where the crowding is quite severe, and we prefer to retain only upper limits for these levels.

In an earlier report (Boissé et al. 2001), we assigned the 1046.45 Å feature to the $v = 4$, $J = 2$ level (line 5 in Fig. 1). This line appears clearly only in the first spectrum and given i) the small f value (6×10^{-3}); ii) absence of other detections from the same level and iii) absence of time variations of clearly detected highly excited H_2 features, this identification appears questionable. Only spectra from the HST/STIS would allow us to unambiguously quantify the amount of H_2 in levels with excitation energies above 10^4 K.

• HI: in our data, the Lyβ line is present although heavily blended with H_2 $J = 0$, 1, 2, 5 absorptions near 1025 Å (Lyγ and Lyδ can also be seen but the *S/N* ratio degrades rapidly at

lower wavelengths and blends are numerous so we use only Lyβ to constrain N(HI)). Thanks to the large width of this Lyβ-H_2 absorption, airglow emission does not affect its profile (emission occurs only in the central part of the trough, where the flux is zero; Fig. 11). To fit the spectrum in this region, we adopt the values for $N(H_2, v = 0, J)$ inferred from other H_2 systems and vary N(HI). The shape of the red edge of the broad 1025 Å trough (around 1027 Å) is primarily due to Lyβ (see Fig. 11) from which we estimate $N(\mathrm{HI}) = 2.7 \times 10^{21}$ cm^{-2}, a value significantly larger than that derived by Mc Lachlan & Nandy 1984 ($N(\mathrm{HI}) = 1.75 \times 10^{21}$ cm^{-2}) from IUE Lyα data taken in 1979. We come back to N(HI) variations in Sect. 5.4.

• HD, $J = 0$: several lines are detected (near 1007, 1011, 1021, 1031, 1042, 1054, 1066 Å) but unfortunately, most of them are either blended, located in regions of poor *S/N* or have an ill-defined continuum. For instance, the strong 1021.456 Å line is expected to be blended with an SII feature with an unknown oscillator strength. The 1031 Å feature is contaminated by an H_2 ($v = 1$, $J = 3$) line for which N is reasonably well determined; OVIλ1031 might also contribute, but this cannot be assessed since the OVIλ1037 line coincides with a damped H_2 line. The 1054 Å line appears much too faint with respect to the others ($W \approx 15$ mÅ); probably, this is due to an ill-defined continuum caused by extra absorption adjacent to this line. In contrast, the 1066.27 Å feature is too strong with respect to the 1031.91 Å one. It is thus difficult to infer a value for N(HD, $J = 0$) consistent with all lines detected. Moreover, N values are strongly dependent on the velocity distribution, which might differ from that of CH. We therefore cannot do better than give an order of magnitude estimate: N(HD, $J = 0$) $\approx 10^{15-16}$ cm^{-2}.

• HD $J = 1$: lines from excited HD have already been detected in the Copernicus spectrum of ζ Oph (Wright & Morton 1979). The strongest feature mentioned by these authors, at 1021.916 Å, is apparently present in our five spectra, although blended with other weak lines. We estimate $W = 8 \pm 2$ mÅ. Other lines of comparable strength are expected from HD $J = 1$; at the position of the 1054.722 Å transition, a strong line with $W \approx 35$ mÅ is present but it is much too strong in comparison to the previous feature and is likely of stellar origin. Finally, around 1043.288 Å (on the blue wing of a H_2 $J = 3$ line) the spectra display large variations which are of instrumental or stellar origin and the search is inconclusive. The tentative detection of the 1021.916 Å line implies $N(\mathrm{HD}, J = 1) = 5.4 \pm 1.3 \times 10^{13}$ cm^{-2}.

• CI: numerous lines from CI and its fine structure excited levels are detected which can be used to measure N(CI), N(CI*) and N(CI**) and get constraints on the density, n. This key parameter has been estimated by Federman et al. (1994) from the analysis of C_2 excitation.

Several combinations of lines from three multiplets were considered between 1129 and 1160 Å; spectral regions containing lines with unknown f values were excluded. Various attempts were made to fit line profiles using OWENS; we successively considered either unblended or unsaturated features alone or all of them together. The instrumental LSF was allowed to vary slightly across the spectrum and b values between 3 and 6 km s^{-1} were considered. The results are the following:

– N(CI) = 9.4 (+ 7.0, –5.8) $\times 10^{15}$ cm^{-2};
– N(CI*) = 5.8 (+ 0.0, –4.2) $\times 10^{15}$ cm^{-2};
– N(CI**) = 2.2 (+ 1.8, –1.1) $\times 10^{15}$ cm^{-2}.

These estimates and uncertainties represent the best compromise we find given our limited knowledge of the LSF and velocity distribution.

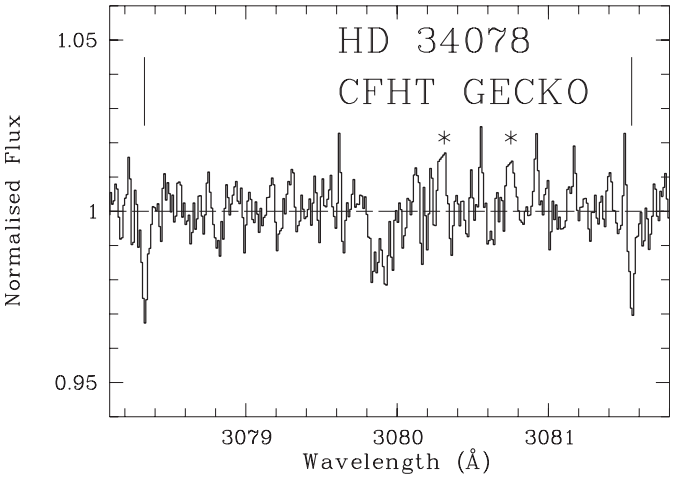

Fig. 4. Portion of the normalised CFHT spectrum comprising two OH absorption lines (indicated by tick marks). The broad absorption around 3079.9 Å is due to a detector defect. High intensity values on two "hot pixels" (noted *) have been cut.

3. The CFHT data

We observed OH absorption lines around 3080 Å from the A-X (0–0) transition band towards HD 34078 with the Canadian-France-Hawaiian telescope. The observations were performed in 2001, October 4–7. We used the GECKO spectrometer, in the UV f/4 Coudé train at a nominal resolving power of $R = 120\,000$. The CFHT EEV1 CCD was used as the detector. The spectrum was cross dispersed by a grism and OH lines appear in the 18th order. An integration time of 14 h provided a *S/N* ratio of 36 per 35 mÅ pixel. Data were reduced in a standard way using the IRAF package. The three OH lines expected in the range covered are clearly detected. An extract is presented in Fig. 4 and equivalent widths are given in Table 3. The inferred OH column density towards HD 34078 is $N(\mathrm{OH}) = 3.5 \pm 0.5 \times 10^{13}$ cm^{-2}.

4. Properties of the gas along the line of sight

In this section, we study physical properties such as excitation, temperature and kinematics. Small scale structure is considered in the next section. We first discuss parameter values as inferred from the analysis of absorption lines measured in the first spectrum and then present a model attempting to account for all known observational constraints.

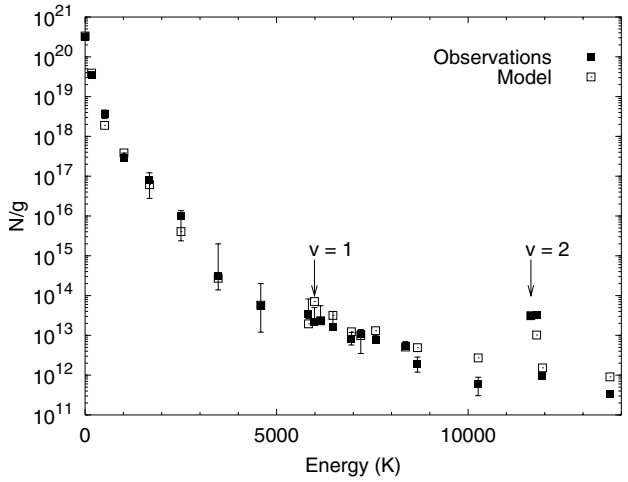

Fig. 5. Observed H_2 excitation diagram (filled squares with 3σ error bars shown; above 11 000 K, observed values are upper limits)) and predictions of the model. The energies of the lowest vibrationally excited $v = 1$, 2 H_2 levels are indicated.

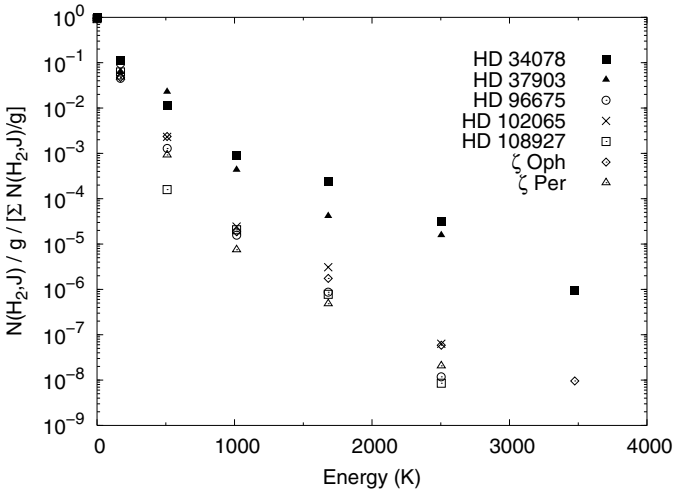

Fig. 6. Comparison of the H_2 excitation diagrams observed for the lines of sight towards HD 34078, HD 37903, HD 96675, HD 102065, HD 108927, ζ Oph and ζ Per. Column densities for the $J = 0$ to 6 levels have been normalised to the total H_2 column density for each line of sight. For HD 102065, the $N(J)$ values correspond to a b value of 3 km s^{-1}.

4.1. Observational results and comparison to other lines of sight

In Fig. 5 we give the excitation diagram corresponding to the estimates or upper limits listed in Table 2.

As observed for other lines of sight, there is a clear flattening as excitation energy increases. The $J = 0$ and 1 values provide a direct measurement of the gas temperature, $T = 77$ K (71–83 K). The slope inferred from the $J = 3$ to 7 values corresponds to $T_{\rm exc} \simeq 360$ K, whereas the detections up to energies of 10^4 K are roughly fitted by $T_{\rm exc} \simeq 1200$ K. No J parity effect is noticeable.

In order to assess whether the H_2 excitation towards HD 34078 differs from the one determined on other lines of sight already at low J (and not only at high excitation energies), we present in Fig. 6 a compilation of results for H_2 levels from $J = 0$ to 6 for HD 96675, HD 102065, HD 108927 (Gry et al. 2002), ζ Oph (Morton 1975) and ζ Per (Snow 1977; the Copernicus data have been reanalysed using new oscillator strength values as described in Le Petit et al. 2004). The first three lines of sight have been chosen because the gas probed is known to be far away from the star.

We also include in Fig. 6 results obtained for HD 37903, the illuminating star of NGC 2023 in Orion. In HST/STIS spectra of that B1.5 V star, Meyer et al. (2001) detect a large amount of highly excited H_2, which is consistent with UV fluorescent excitation of dense molecular gas located close to HD 37903. The data shown in Fig. 6 for $J \leq 6$ are from ORFEUS observations (Lee et al. 2002).

For the purpose of comparison, column densities have been normalised to the total H_2 column density appropriate for each line of sight. It is clear in Fig. 6 that for the two lines of sight in which strong absorption from excited H_2 is detected (from $J \geq 8$), HD 34078 and HD 37903, the excitation excess is already apparent at $J = 2$ with respect to other, more "standard", lines of sight. Beyond $J = 3$, the excess attains two orders of magnitude. In contrast, the relative amount in the $J = 1$ level (corresponding to $T \approx 77$ K towards HD 34078) is quite consistent with other measurements.

Apart from the detections presented in this paper, several other molecular species have been observed towards HD 34078 which can be used to constrain a physical/chemical model of the gas: C_2 (Federman et al. 1994), CH, CH^+, CN (Rollinde et al. 2003) and CO (Mac Lachlan & Nandy 1984). The corresponding column densities are summarized in Table 4. It appears that, on one hand, column densities of molecular species as well as the H_2 temperature, T_{01}, are qualitatively similar to those found on other lines of sight and, on the other hand, the H_2 excitation above $J = 2$ is unusually high compared to that in standard diffuse ISM. This suggests the presence of two distinct components along the line of sight: i) "quiescent" gas within a translucent cloud, responsible for the absorption due to H_2 $J = 0$ and 1 and to other molecular species and ii) gas located close to HD 34078 dominating absorption from H_2 at $J > 2$.

The HI/H_2 ratio only provides a lower bound for comparison with model predictions since diffuse HI not associated to molecular gas is likely to be present along the line of sight. Adopting the N(HI) value derived from our FUSE observations, the resulting total hydrogen column density along the line of sight, $N(\mathrm{H}) = N(\mathrm{HI}) + 2\,N(\mathrm{H_2})$, is 3.3×10^{21} cm^{-2}. Given the $E(B-V)$ value quoted in Table 1, the implied $N(\mathrm{H})/E(B-V)$ ratio is consistent with the value measured by Bohlin et al. (1978).

4.2. Modelling

To investigate the ability of our model to reproduce observed column densities we use a recent version of the PDR model of Le Bourlot et al. (1993) as well as the MHD shock model of Flower & Pineau des Forêts (1998), updated for diffuse clouds and including explicit rotational excitation of H_2. As described in Le Petit et al. (2002), the PDR model features a

Table 1. Properties of the line of sight. Right side of the chart: extinction curve coefficients.

Spectral Type[(1)]	O9.5Ve	Ext. curve[(4)]	
$\alpha^{(1)}$ ($J2000$)	05 16 18.15	c_1	0.473
$\delta^{(1)}$ ($J2000$)	+34 18 44.3	c_2	0.571
$m_v^{(1)}$	5.998	c_3	4.152
parallax[(1)] (mas)	2.24	c_4	0.52
$E(B-V)^{(2)}$	0.52	γ	1.087
$R_v^{(3)}$	3.42	x_0	4.589

(1) Simbad database.
(2) Crawford (1975).
(3) Patriarchi et al. (2001).
(4) Fitzpatrick and Massa (1990).

plane-parallel slab of gas and dust illuminated on one side by a UV radiation field. The radiative transfer as well as the thermal balance are calculated (the temperature can also be fixed, if derived from observations). The J dependent photodissociation of molecules such as H_2 and HD as well as their excitation in ro-vibrational levels due to radiative excitation, decay and collisional excitation are computed. About 100 chemical species linked by a network of 1400 chemical reactions have been taken into account. The elemental abundances and dust size distribution used here are those given in Le Petit et al. (2002). Note that while the extinction curve effectively measured towards HD 34078 is used to describe the attenuation of the UV field, the dust size distribution adopted is consistent with the average Galactic extinction curve. The main properties of the line of sight (extinction curve and R_v value) are given in Table 1. The density and intensity of the incident radiation field in each of the two components are adjusted to reproduce the observed H_2 excitation as well as the amount of other molecules. Column densities are computed through integration of the local abundances given by the model, assuming a face-on geometry.

4.2.1. The transluscent cloud

For the translucent cloud we assume an incident radiation field equal to that in the solar neighborhood as estimated by Draine (1978). An isothermal model is adopted at $T = 77$ K, the kinetic temperature from the two first H_2 levels. The gas density is well constrained by absorption from the first three CI levels. Trying several values for $n_{\rm H}$, models with densities of 600 cm^{-3} and below appear to underestimate N(CI) whereas those with $n_{\rm H} \geq 800\,{\rm cm}^{-3}$ overestimate $N(\rm CI^*)$. We adopt $n_{\rm H} = 700\,{\rm cm}^{-3}$ as the best compromise. With these parameters, integrating abundances to match the observed $N(H_2, J = 0)$ and $N(H_2, J = 1)$, we find that column densities of all other molecules (excepted CH^+ and OH discussed below) are well reproduced given the measurement uncertainties and the small number of free parameters in the model (cf. Table 4). The visual extinction corresponding to this component is $A_{\rm v} = 0.8$.

To account for the CH^+ abundance we add to the PDR component a C-shock with a velocity $v = 25\,{\rm km\,s}^{-1}$, a pre-shock density of 20 cm^{-3} and a magnetic field of 7 μG. The shock contributes only slightly to the excitation of H_2 for levels $J = 5$ to $J = 7$ (Fig. 7). The thickness of the shocked layer corresponds to $A_{\rm v} \approx 0.1$ and gives a negligible contribution for other species, OH excepted. In this latter case, the contribution of the MHD shock is too large by a factor of about 7 (Table 4). The maximum temperature of neutral species reached in the shock is 4000 K. A single shock has been used here; vortices or a collection of several weaker shocks could have been considered as well to represent the dissipation of kinetic energy along the whole line of sight (cf. Gredel et al. 2002), which might help to reduce the discrepancy between the observed and model N(OH) values. However, since the C-shock required to account for $N(CH^+)$ appears to play no important role for the H_2 excitation, no further attempt to fit both the observed OH and CH^+ values was made (OH observations are relatively scarce due to the wavelength range of its absorption lines and thus little is known about correlations between OH and CH^+).

4.2.2. The hot PDR around HD 34078

The contribution of material surrounding HD 34078 is strongly suggested not only by the anomalous excitation diagram but also by the IRAS detection of a far infrared excess associated with this star by van Buren et al. (1995). According to these authors, such an emission is indicative of a bow shock located around the star, at the interface between the stellar wind and the ambient interstellar medium, where the material is strongly compressed. In this location, dust grains are exposed to an intense UV field and emit FIR radiation, accounting for the excess observed in IRAS data. We shall assume in the following that a scenario like the one proposed by Mac Low et al. (1991) to describe cometary compact HII regions also applies in our case and that H_2 is present in a thin layer within the bow shock (cf. their Fig. 2). This is not obvious here since the ambient medium is not necessarily dense enough to contain H_2 molecules (this point is discussed in Sect. 4.2.3). Below, we consider this bow shock as a PDR and show that excitation of the H_2 molecules by UV photons can explain the observed excitation.

Since we have no observational constraints on the temperature for this component, we now consider models in which the thermal balance equation is solved. The density n and the intensity of the incident radiation field χ expressed in Draine's units are varied so as to reproduce the H_2 excitation diagram. We find that adopting $n_{\rm H} = 10^4$ cm^{-3}, $\chi = 10^4$ and integrating abundances up to $A_{\rm v} = 1.0$, we get a remarkably good fit given the limited number of free parameters, as illustrated in Figs. 5 and 7. H_2 column densities for levels $J = 3$ and above are correctly reproduced, indicating that the hot PDR naturally accounts for both the overpopulation measured for $J \geq 3$ and the high energy tail (beyond $J = 7$) not seen in most lines of sight (let us recall that N values are well constrained by observations both for $J = 3$ and $J \geq 8$ since in these two limits W no longer depends on b). Then, the "standard" H_2 $J = 2$ to 7 population as shown in Fig. 6 is masked on this particular line of sight by the hot PDR component. Most of the observed atomic hydrogen comes from this component. Because of the high radiation field, column densities of molecules like CO, CH, OH etc. are

Table 2. Measured column densities for various H_2 levels (best estimate and 3σ lower and upper bounds) and predictions from our model (see text). The number of lines effectively used in the determination of $N(H_2, v, J)$ is given as M_l.

					Observations			Modelling			
v	J	g	Energy (K)	M_l	$N(H_2, v, J)$ (cm^{-2})	Lower limit	Upper limit	Transluscent Cloud	C-shock	hot PDR	Total
0	0	1	0	5	3.2(20)	3.0(20)	3.6(20)	3.2(20)	8.6(17)	2.1(18)	3.2(20)
0	1	9	170	10	3.2(20)	2.9(20)	3.5(20)	3.2(20)	3.1(18)	1.4(19)	3.4(20)
0	2	5	510	3	1.8(19)	1.4(19)	2.3(19)	2.0(18)	4.4(17)	4.0(18)	6.4(18)
0	3	21	1015	5	6.2(18)	5.5(18)	8.0(18)	6.1(15)	6.5(17)	6.0(18)	6.7(18)
0	4	9	1682	4	7.1(17)	2.5(17)	1.1(18)	2.0(14)	7.0(16)	5.5(17)	6.2(17)
0	5	33	2504	4	3.3(17)	7.8(16)	4.5(17)	7.6(13)	4.7(16)	1.9(17)	2.4(17)
0	6	13	3474	5	4.0(15)	1.8(15)	2.6(16)	8.4(12)	2.8(15)	3.6(15)	6.4(15)
0	7	45	4586	1	2.5(15)	5.4(14)	9.0(15)	7.5(12)	1.4(15)	2.0(15)	3.4(15)
0	8	17	5830	5	6.0(14)	4.5(14)	1.4(15)	1.1(12)	9.1(13)	2.5(14)	3.4(14)
1	0	1	5987	2	2.2(13)	2.0(13)	5.0(13)	2.7(11)	1.4(12)	2.9(13)	3.1(13)
1	1	9	6150	2	2.1(14)	1.7(14)	5.0(14)	7.7(11)	1.2(13)	1.4(14)	1.5(14)
1	2	5	6472	3	8.3(13)	7.0(13)	2.0(14)	6.8(11)	5.1(12)	9.8(13)	1.0(14)
1	3	21	6952	4	1.7(14)	1.2(14)	2.5(14)	6.9(11)	1.5(13)	1.8(14)	2.0(14)
0	9	57	7197	8	6.0(14)	2.0(14)	8.0(14)	1.5(12)	4.6(13)	4.5(14)	5.0(14)
1	4	9	7585	4	7.0(13)	6.0(13)	9.0(13)	3.0(11)	4.1(12)	8.0(13)	8.4(13)
1	5	33	8365	3	1.8(14)	1.5(14)	2.3(14)	2.4(11)	7.9(12)	1.2(14)	1.3(14)
0	10	21	8677	2	4.0(13)	2.5(13)	6.0(13)	2.5(11)	3.6(12)	8.1(13)	8.5(13)
0	11	69	10262	3	4.1(13)	2.1(13)	6.1(13)	4.1(11)	1.8(12)	1.5(14)	1.5(14)
2	0	1	11636	1	–	–	3.0(13)	1.1(11)	1.9(10)	1.3(13)	1.3(13)
2	1	9	11789	1	–	–	3.0(14)	3.0(11)	1.6(11)	6.1(13)	6.1(13)
0	12	25	11940	2	–	–	2.4(13)	7.5(10)	1.5(11)	3.1(13)	3.1(13)
0	13	81	13703	1	–	–	2.7(13)	1.4(11)	–	6.2(13)	6.2(13)

Table 3. Equivalent widths and column densities derived from the OH transitions observed towards HD 34078. Wavelengths and oscillator strengths are taken from Felenbok & Roueff (1996).

	Transitions (0-0) X-A		
λ_{air}	3072.0105 + 3072.0637	3078.4399 + 3078.4720	3081.6645
Transition	$R_1(3/2) + {}^RQ_{21}(3/2)$	$Q_1(3/2) + {}^QP_{21}(3/2)$	$P_1(3/2)$
f	4.55(–4)	1.05(–3)	6.48(–4)
W (mÅ)	≤1.0	1.72 ± 0.27	0.86 ± 0.21
N (cm^{-2})	$\leq 2.6 \times 10^{13}$	$1.9 \pm 0.3 \times 10^{13}$	$1.6 \pm 0.4 \times 10^{13}$

negligible as compared to those of the translucent component due to large photodissociation rates (cf. Table 4).

By varying n and χ around the best fit values, we find that the density is well constrained by the model: with $\chi = 10^4$, the amount of high excitation H_2 can be reproduced only with n_H between 5000 and 5×10^4 cm^{-3}. On the other hand, the intensity of the radiation field is poorly constrained. For a density $n_H = 10^4$ cm^{-3} it is possible to reproduce the H_2 excitation diagram without exceeding the observed N(H I) and $N(H_2)$ with χ between 500 and 10^4. We thus find that a two-component model (complemented by a C-shock to account for CH^+ production within the translucent cloud) successfully reproduces the main characteristics of the gas along the line of sight towards HD 34078.

A comparison of the excitation diagrams obtained for HD 34078 and HD 37903 (Figs. 6, 7 and 2 from Meyer et al. 2001) indicates that they are relatively similar. Moreover, it is noteworthy that the amounts of H_2 and dust are comparable on these two lines of sight: $N(H_2) = 6.4 \times 10^{20}$ and 7.8×10^{20} cm^{-2} and $E(B-V) = 0.52$ and 0.35 for HD 34078 and HD 37903 respectively (the spectral types are also close to each other: O9.5V and B1.5V). It is then not surprising that when modelling the high energy part of the HD 37903 diagram, Meyer et al. (2001) derive values for the radiation field and gas density consistent with our estimate for the hot PDR component around HD 34078. In our picture, the markedly different proper velocities of these two stars (only HD 34078 is a runaway) could just correspond to distinct mechanisms responsible for the presence of high density gas close to each star.

4.2.3. Discussion

As already noted, we adopted in the above model the true HD 34078 extinction curve but a dust size distribution corresponding to the average Galactic extinction curve. This lack of consistency could have significant effects on model results. To estimate the uncertainties related to the (unknown) dust size distribution, we ran additional models using the average Galactic extinction curve (including the appropriate R_v value) instead of the HD 34078 one and imposing similar values as

Table 4. Observed and computed column densities in cm^{-2}.

	Observations			Modelling			
	Observations	Min. Val.	Max. Val.	Transluscent Cloud	C-shock	hot PDR	Total
$H^{(1)}$	2.7×10^{21}	2.2×10^{21}	3.4×10^{21}	2.6×10^{19}	1.2×10^{19}	1.7×10^{21}	1.7×10^{21}
$H_2{}^{(2)}$	6.4×10^{20}	6.0×10^{20}	6.9×10^{20}	6.5×10^{20}	5.1×10^{18}	2.7×10^{19}	6.8×10^{20}
A_V	1.8			0.8	0.1	1.0	1.9
$HD^{(2)}$		10^{15}	10^{16}	8.5×10^{15}	–	5.4×10^{13}	8.5×10^{15}
$CH^{(3)}$	9.5×10^{13}	9.3×10^{13}	1.1×10^{14}	5.0×10^{13}	4.1×10^{12}	7.4×10^{9}	5.4×10^{13}
$CH^{+(3)}$	6.5×10^{13}	5.8×10^{13}	7.1×10^{13}	1.9×10^{10}	6.0×10^{13}	5.0×10^{11}	6.0×10^{13}
$C_2{}^{(4)}$	5.8×10^{13}	–	–	2.3×10^{13}	2.9×10^{10}	1.4×10^{7}	2.3×10^{13}
$C_3{}^{(5)}$	2.2×10^{12}	1.7×10^{12}	2.7×10^{12}	7.2×10^{11}	–	1.3×10^{3}	7.2×10^{11}
$OH^{(2)}$	3.5×10^{13}	1.4×10^{13}	5.6×10^{13}	1.4×10^{13}	2.5×10^{14}	5.9×10^{11}	2.6×10^{14}
$CN^{(4)}$	3.3×10^{12}	–	–	1.6×10^{12}	5.8×10^{11}	4.8×10^{8}	2.2×10^{12}
$CO^{(6)}$	5.7×10^{14}	4.6×10^{14}	7.2×10^{14}	1.1×10^{15}	3.0×10^{13}	1.1×10^{11}	1.1×10^{15}
$CI^{(2)}$	9.4×10^{15}	3.6×10^{15}	1.7×10^{16}	3.5×10^{15}	–	2.4×10^{12}	3.5×10^{15}
$CI^{*(2)}$	5.8×10^{15}	1.6×10^{15}	5.8×10^{15}	5.7×10^{15}	–	6.9×10^{12}	5.7×10^{15}
$CI^{**(2)}$	2.2×10^{15}	1.1×10^{15}	4.0×10^{15}	2.8×10^{15}	–	1.0×10^{13}	2.8×10^{15}

Dash means an unknown value.
Last column (Total) corresponds to the sum of the components in the model.
References for the observations are:
(1) This work and Mc Lachlan & Nandy (1984).
(2) This work.
(3) Rollinde et al. (2003).
(4) Federman et al. (1994), Rollinde et al. (2003).
(5) Oka et al. (2003).
(6) Mc Lachlan & Nandy (1984).

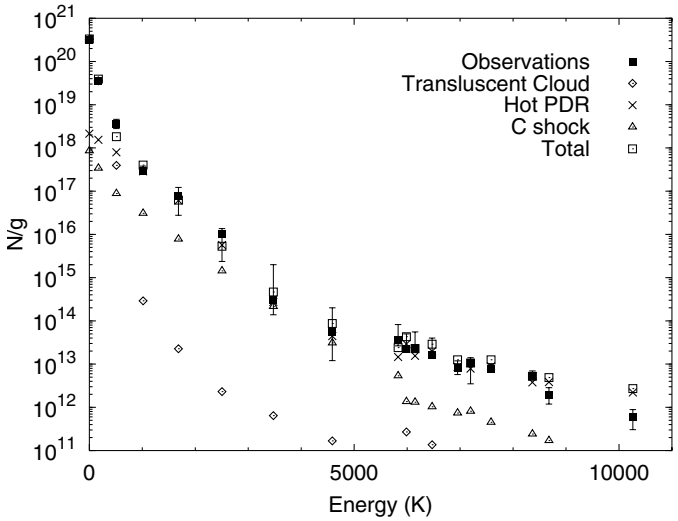

Fig. 7. Observed H_2 excitation diagram and H_2 column densities for each of the three components in the model.

those given in Table 4 for the H_2 column density of the translucent cloud and hot PDR components. We find that the results of both models remain within the observational uncertainties; in the H_2 excitation diagram, the maximum difference in $N(H_2, v, J)$ is less than 25% and similarly small relative variations are seen for the abundances of species like CI, CH, CN (the variation attains 50% for CO). We then conclude that our model results are not strongly dependent on the adopted dust size distribution and that the good agreement with observations is fully significant.

In order to better assess the reliability of the hot PDR component, one can estimate from dynamical arguments the distance of the bow shock to the star and infer the corresponding radiation field intensity. Using Eq. (2) from van Buren et al. (1990), adopting an average density of the ambient ISM of $n_a \simeq 1\ cm^{-3}$ and a star velocity of $100\ km\,s^{-1}$, we get a distance of $d_s \simeq 0.5$ pc. Considering the observed flux of HD 34078 at $\lambda \simeq 1100$ Å (10^{-11} erg cm^{-2} s^{-1} Å^{-1}) and correcting for the dust attenuation implied by $E(B-V) = 0.5$ and the observed extinction curve ($\tau_{1100} = 6.3$), we find that the distance d_{rad} at which the intensity of the radiation field of the star is equal to 10^4 times the ISRF is 0.2 pc, approximately the estimated distance of the shock to HD 34078. This good agreement gives coherence to our model. An additional test would consist in estimating the density of the material located in the bow shock, but unfortunately this is strongly dependent on the magnetic field and the shock velocity (both unknown).

Although the spectral resolution is limited, one can also use the absorbing gas kinematics to test our model. In the latter, all

H_2 absorptions from levels above the $J = 2$ one arise from the same component, the hot PDR. These lines should therefore be characterized by a common velocity. To search for a possible Doppler shift among $J \geq 3$ lines we selected spectral regions with good *S/N* ratio and displaying $J = 3$, 4, 5 lines with closeby $J = 9$ absorptions. Similarly, around 1059 Å, a group of 7 H_2 lines from $v = 0$, $J = 4$, 6, 7, 8 and $v = 1$, $J = 3$, 4 is present. In all these cases, we find that the r.m.s. scatter in wavelength shifts is no larger than 0.005 Å, which implies a velocity difference smaller than 1.5 km s^{-1} (or about 5 km s^{-1} at 3σ).

Conversely, since the translucent and hot PDR components are unrelated in our model, their velocity distributions should differ both in the average and width, unless they happen to coincide by chance. $J = 0$ and 1 absorptions are too broad to provide any valuable velocity estimate. We can use instead HD lines which trace the same component. Near the 1031 and 1054 HD $J = 0$ absorptions, we find a few narrow H_2 absorptions (from the hot PDR component) and by comparing measured wavelengths to the laboratory values, we find no significant shift between the two components to a similar limit as above (5 km s^{-1} at 3σ). The test is however not so constraining because the number of measurements is limited and the accuracy of the latter is difficult to assess because i) the continuum is uncertain and ii) unrecognized blends may be present. Regarding velocity dispersions, one would expect a priori a larger value for disturbed gas near HD 34078 (i.e. the hot PDR component) than for the foreground translucent cloud. High resolution observations of CH absorption can be used to probe the latter, which indicates $b \approx 3$ km s^{-1} (Allen 1994; Rollinde et al. 2003). As discussed in Sect. 2.2, there is no clear evidence for a significantly larger dispersion in high excitation gas. Thus, tests involving kinematics do not provide additional support for our two-component model.

The similarity of the velocity and velocity dispersions of the two components suggests that perhaps the latter are not unrelated. The suggestion made by Herbig (1958) is interesting in this regard. Based on a comparison of Hα and visible continuum images, he proposed that HD 34078 has recently encountered new cloud material. In such a scenario, one can imagine that the density of the ambient medium, n_a, is about 10–20 cm^{-3} instead of 1 cm^{-3}. A first consequence involves the origin of the excited H_2. With $n_a \simeq 1$ cm^{-3}, H_2 molecules would not preexist and would need to be formed in the bow shock; we estimate that at $n \simeq 10^4$ cm^{-3}, 10^5 yrs are required while it takes no longer than 10^4 yrs (a few 0.2 pc/100 km s^{-1}) for the compressed material to drift from the head of the shock to the sightline (after 10^4 yrs, the fraction of molecular H_2 is less than 10% of its steady-state value). In contrast, if $n_a \simeq 20$ cm^{-3}, H_2 can be supposed to be already in place in the ambient medium. Moreover, applying mass conservation for the swept gas leads to a predicted H_2 column density through the hot PDR which is consistent with the observed one. Indeed, one gets the relation $\pi R^2 \cdot n_a = 2\pi \cdot R \cdot \Delta R \cdot n_{PDR}$ or $n_a \cdot R = 2 \cdot \Delta R \cdot n_{PDR} = 2N_{PDR}$ where R is the radius of the cylinder containing the swept material (which we assume to be comparable to d_s), ΔR the thickness of the PDR, n_{PDR} and N_{PDR} the density and column density throughout the compressed layer. We find that N_{PDR} is of the order of 10^{19} cm^{-2}, comparable to the column density estimate for the hot PDR drawn from our best fit model (Table 4). Finally, in a denser ambient medium the shock will occur closer to the star (d_s goes as $n_a^{-0.5}$) and with $n_a \simeq 20$ cm^{-3}, $d_s \simeq 0.1$ pc (instead of 0.5 pc for 1 cm^{-3}), quite comparable to d_{rad}. Thus, a relatively high density for the ambient medium around HD 34078, as suggested by Herbig (1958), appears to be well consistent with the modelling of the H_2 excitation.

One question that remains open is the relation between the translucent component containing the bulk of the H_2 ($J = 0$, 1) and the hot PDR material. The low temperature (77 K) of the H_2 gas, the low velocity dispersion as estimated from CH and the presence of many molecules that might be photodissociated if located too close to HD 34078 suggest that the translucent cloud is not associated to the star. In contrast, the similarity of velocities and velocity dispersions favors a picture in which the two components have a common origin. Below (Sect. 6), we propose a few observations which should help to clarify the relation between HD 34078 and the bulk of the molecular gas.

5. Absorption line variations and small scale structure towards HD 34078

The original purpose of our project was to probe the structure of quiescent molecular gas. The discovery of high excitation H_2, making the line of sight towards HD 34078 somewhat peculiar, could have been embarrassing. However, the modelling work described above indicates that absorption from the $J = 0$ and 1 H_2 levels (which comprise by far most of the gas) traces material unperturbed by HD 34078. In the following, we first search for variations in the damped line profiles from these two levels, which can be used to investigate in a direct and efficient way column density variations, regardless of any assumption on the velocity distribution. The five spectra available span a time interval of 2.7 yr, which corresponds to linear scales of about 50 AU in the foreground cloud.

In our model, lines from all other H_2 levels originate essentially from gas surrounding HD 34078. Since the compressed material is continuously flowing across the line of sight as the star moves, the time behavior of these lines should tell us whether this flow is regular or chaotic. Further, if there exist density fluctuations in this gas or changes in the UV field, this should also result in variations of absorption lines arising from the hot PDR component. In order to select those H_2 levels that display the highest sensitivity to changes in n or χ, we use the model presented in Sect. 4. We vary the density, n, and radiation field, χ, (separately) by a factor of 2, and find that the sensitivity to changes in χ is small for all levels (30% at maximum for $J = 4$–5), while the response to similar variations in n is much larger with a peak at $J = 6$. $N(J = 6)$ varies by a factor of 3.4, and beyond $J = 8$ the induced variation in $N(v, J)$ is around 50%, relatively independent of the level. Unfortunately, absorptions from levels $J = 5$, 6, 7, 8 are heavily saturated and the observed profiles or W values are weakly dependent on $N(J)$ (these lines can be used instead to assess the stability of the instrument). We shall then examine the good *S/N* lines

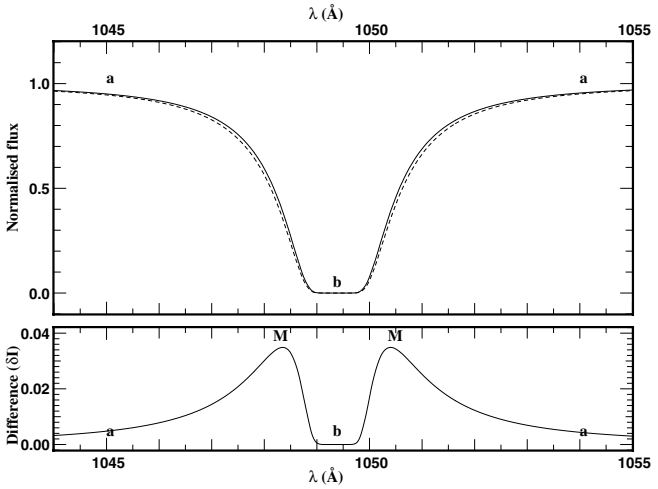

Fig. 8. Profile variation for the H_2 Lyman (4–0) R(0) 1049.37 Å transition. *Top panel*: the solid line corresponds to $\log(N) = 20.6$. The dashed profile is obtained by varying N by +10%. *Lower panel*: difference between the two profiles. In both panels, regions noted **a)** and **b)** are subject to little variation which implies the presence of a maximum (**M**) in between.

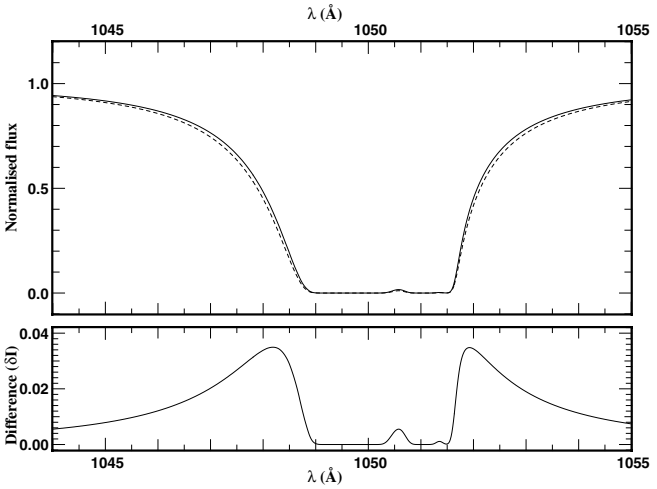

Fig. 9. Same as in Fig. 8 but for the whole blend of $J = 0$, 1, 2 lines ((4–0) Lyman band). The assumed variation is $\delta N/N = 10\%$ for each of these three levels.

with intermediate opacity ($\tau \approx 1-3$) arising from high excitation levels ($J \geq 9$).

In Boissé et al. (2001), we presented a report based on the first three spectra, among which no significant changes were noted, except a possible variation of lines from highly excited H_2.

5.1. Sensitivity of absorption lines to column density variations

The sensitivity of an absorption line profile to small column density variations can be estimated from the ratio $Q \equiv (\delta I/I_c)/(\delta N/N)$, where I is the *observed* profile and I_c the continuum. Considering ideal Voigt profiles observed at a given finite resolution, Rollinde (2003) has shown that a good sensitivity is achieved in two cases: i) fully resolved lines (e.g. damped H_2 absorption from low J levels) and ii) marginally thin lines (central opacity, $\tau_0 \approx 1$).

Consider an unblended and fully resolved damped line. If the column density increases the profile broadens, which results in a decrease of I/I_c at any given wavelength, except in the line core and outside the wings where $I = I_c$ (Fig. 8). It can be shown that the Q parameter reaches its maximum, $Q_{max} = 0.357$, on each wing of the profile at wavelengths where the optical depth τ_0 equals 1 and $I/I_c = 0.37$ (Rollinde 2003). For a change of N by 10%, the expected variation in I/I_c is 0.035 (well above the noise level in our FUSE spectra). The corresponding broadening of the profile at $\tau_0 = 1$ on each wing is typically 0.05 Å (a value comparable to the resolution).

A damped profile corresponds to

$$I = I_c \exp\left(-\left[\frac{6.726 \times 10^{-17}}{c^2}\right] \times \frac{N f \lambda_0^2 \gamma}{(\lambda_0/\lambda - 1)^2}\right)$$

where c is the light velocity (in km s^{-1}), f the oscillator strength, γ the radiative rate (in s^{-1}), and where λ_0 and N are expressed in Å and cm^{-2} respectively. Then, if variations are observed for one specific line, one can predict exactly the corresponding variations expected for other damped lines from the same level. This gives a powerful method for checking the reality of any variation and rule out artefacts of instrumental origin (e.g. due to distortions in the wavelength calibration).

In practice, the low J H_2 transitions in FUSE spectra appear in "systems", where one $J = 0$, two $J = 1$ and one $J = 2$ lines are strongly blended (e.g. for the (4–0), (3–0) and (2–0) Lyman bands at $\lambda \approx 1050$ Å, 1063 Å, 1078 Å respectively). To compute the expected variation of the whole system profile, we assume that the excitation of the gas is uniform i.e. that the relative variations of $N(J = 0)$, $N(J = 1)$ and $N(J = 2)$ are identical. Comparison of synthetic profiles corresponding to values of $N(J = 0$, 1 and 2) similar to those given by profile fitting of the FUSE spectra indicates that the blue wing of the $J = 0$ line and the red wing of the $J = 2$ line in each system (the two extreme transitions of the blend) are relatively little affected by the $J = 1$ transitions (Fig. 9). For the 1050 Å H_2 system, changes in $N(J = 1)$ alone result in profile variations that would not be easy to detect because they appear in the far wings of the blend; as a consequence, no useful constraint can be obtained for $N(J = 1)$ from that system.

5.2. Comparison of H_2 damped profiles obtained between Januray 2000 and October 2002

To search for variations among the observed spectra one could fit each system profile (or fit them simultaneously) and then compare the $N(J = 0, 1, 2)$ values obtained for each epoch. However, the accuracy of individual N values would then be strongly limited by our knowledge of the stellar continuum, which is poor given the large width of the H_2 absorptions and high number of additional absorption lines present. A great advantage of *reobserving the same star* is that variations can be searched for through a direct comparison of the spectra themselves.

Before performing this comparison, we need to adjust the wavelength and flux scales of the two spectra considered. These two tasks are performed separately for each H_2 system, on an extract of the spectra centered on the absorption and covering about 15 Å. Using narrow absorption lines located on both sides of the broad absorptions, the wavelength shift to be applied is measured. Similarly, a multiplicative factor bringing the adjacent continua of the two spectra to the same level is determined. In fact the "adjacent continuum" is not easy to define because the various systems overlap, and given our $N(H_2, J)$ values for $J = 0, 1, 2$ the entire spectral domain of interest is affected by H_2 absorption. Thus, to perform the relative flux normalisation, we use regions where H_2 absorption is minimum, about 7 Å away from the center of each trough (e.g. near 1043, 1057, 1071 Å). It is to be noted that such a procedure is approximate only, because a variation in $N(H_2)$ will slightly affect the continuum level, and imposing the same continuum value in the two spectra to be compared will result in an apparently lower variation. However, in our case, the absorption in between two H_2 systems is no larger than about 10%. By applying the internormalisation procedure described above to synthetic spectra with $N(H_2, J)$ differing by 10%, we find that the apparent reduction in the N variation is not really significant, given our accuracy. In the following, we therefore ignore this difficulty.

These two corrections (involving two values only for a given H_2 system and pair of spectra) account i) for unknown changes in the zero-point of the FUSE spectra from one epoch to another (and possibly, for inaccuracies in the FUSE wavelength calibration) and ii) for stellar flux variations (and/or variations in the flux calibration). The second correction assumes that no variation in the spectral shape of the continuum has occurred, which appears consistent with the data (except blueward of the OVI doublet where impressive variations of the absorption due to the stellar wind are seen). As shown in Fig. 10, the superposition is excellent once the two corrections are applied, which indicates a very good instrumental stability.

Variations of the H_2 systems among all spectra have been examined (see Boissé et al. 2001 for a comparison of the first and third spectra). Here, we present results involving the first and fifth spectra, which provide the largest timebase. The comparison has been performed for each of the three 1050, 1063 and 1078 Å H_2 systems. In Fig. 10 we can see that the difference near the red or blue end of the through where the largest variations are expected is no larger than a few percent of the continuum (windows of width ≃0.3 Å are considered) and that no systematic trend towards an increase or decrease of $N(H_2)$ is noticeable (the curves shown in the lower panel are for $N(H_2)$ changes by ±10%). For systems other than those around 1050, 1063 and 1078 Å, the *S/N* ratio is too low or the presence of additional absorption strongly alters the H_2 profile in the spectral regions where the largest variations are expected for I/I_c; in particular, we exclude the 1037 Å system which is affected by variable OVI absorption from the stellar wind.

Very recently (september 2003), we obtained a sixth FUSE spectrum which brings the time interval and scale covered to 3.7 yr and 63 AU respectively. Although these data have not been fully analysed yet, we could verify that the profiles

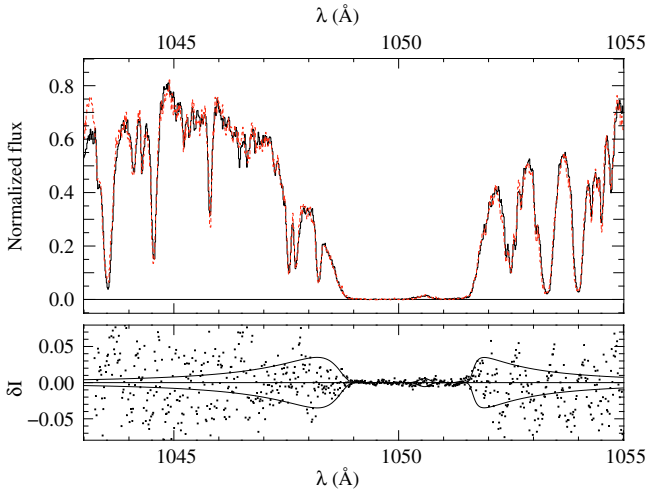

Fig. 10. Comparison of the January 2000 and October 2002 HD 34078 FUSE spectra in the region comprising the 1050 Å H_2 system. *Top panel*: superposition of the normalised spectra (solid line: Jan. 2000; dashed line: Oct. 2002), after applying the corrections discussed in the text. *Lower panel*: the difference between the two observed normalised profiles. The solid lines indicate the expected variation of the H_2 absorption profile for a change $\delta N/N = \pm 10\%$ of the column density for each of the $J = 0$, 1 and 2 levels.

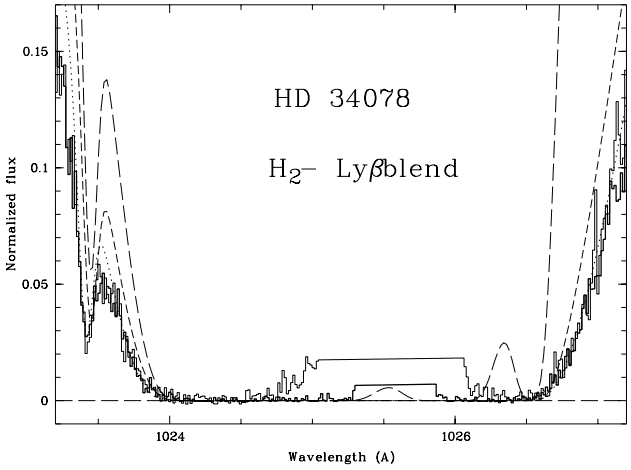

Fig. 11. The bottom of the H_2–Lyβ trough near 1025 Å. The normalized January 2000 (thick line) and October 2002 (thin line) are shown together with synthetic profiles obtained assuming $N(\mathrm{HI}) = 0$ (long-dashed line), $\log(N(\mathrm{HI})) = 21.30$ (the value inferred from 1979 IUE Lyα data; short-dashed line) and $\log(N(\mathrm{HI})) = 21.44$ (our best value; dotted line). Note how the latter value improves the fit on both edges of the trough. The line at 1023.4 Å is from H_2 $J = 4$. The $N(H_2)$ values for $J = 0$, 1, 2, 4 used to compute profiles are those given in Table 2. The emission feature cut out near 1025.5 Å on both spectra is terrestrial Lyβ.

of the three H_2 systems considered above are again completely consistent with those of the earlier epochs.

We thus detect no appreciable change in the damped H_2 profiles. To get an upper limit on column density variations, we shall use a Maximum Likelihood Estimator (as described in Numerical Recipes, Sect. 15.1). The data correspond to the flux variations along the profile of the three systems mentioned above, while column density variations are the parameters to

be determined. For simplicity, we shall consider that H_2 excitation among the $J = 0$, 1 and 2 levels is uniform, i.e. constant in time (clearly, local changes in the excitation would constitute a second order effect). In this assumption, the observed profiles that are blends of absorption lines arising from these three levels depend only on one single parameter, the total (or relative) N variation.

The *likelihood* of δN given a flux variation δI is a function of the wavelength, written as $P(\delta N|\delta I, \lambda)$. This probability distribution is computed from random realisations of synthetic spectra with different column densities (using our fit to the data as a reference) to which we add white noise with an r.m.s. scatter similar to that measured in the observed spectrum. Then, we get the combined *likelihood* function $P(\delta N|\delta I)$ for the set of three H_2 systems quoted above by computing the normalised product of the three individual distributions. The data imply $\delta N/N = 0.02 \pm 0.01$, which corresponds to 3σ lower and upper bounds, $-1\% < \delta N/N < 5\%$.

Observations of the CH and CH^+ blue lines have suggested possible correlated variations of N(CH) and $N(CH^+)$ (Rollinde et al. 2003) on the scale of about one year. One may then wonder in case these fluctuations are real (additional observations are in progress to check this), whether they are accompanied by similar $N(H_2)$ variations. It turns out that, for two CH measurements which display the largest variation in W(CH λ4300) (+6.3% between January 2000 and February 2001 corresponding to + 9.5% in N(CH)), there exist nearly simultaneous FUSE observations (to within a few days). We then examined carefully the 1050 Å H_2 system (which provides the tightest constraints) and searched for any hint of an *increase* in $N(H_2)$ between the two epochs. No such change can be seen and by comparing synthetic profiles obtained by slightly varying $N(H_2, J = 0, 1, 2)$ about the best fit values we find that an increase of $N(H_2)$ as large as 9.5% is clearly ruled out by our data.

Let us conclude this section by a few comments on some systematic effects that might affect the analysis described above. For instance, slight distortions in the wavelength scale could, if large enough, mimic the kind of signature we are searching for (a shift of the blue or red end of the H_2 troughs). Local fluctuations in the continuum level due to varying stellar absorption lines could also induce apparent H_2 absorption changes. However, among the three systems considered these effects are found to be negligible, as indicated by the good agreement between the wavelength shifts derived from various narrow lines adjacent to each system. If future observations were to suggest real variations, we note that the spectral shape of the expected variation could be used to recognize these effects; moreover, data from other detectors (such as LiF2B, which covers in part the same range as LiF1A) could be used also (although of lower *S/N* ratio) to rule out instrumental effects.

5.3. Lines from highly excited H_2

We now search for variations among the low optical depth lines arising from high H_2 levels and tracing (in our model) the hot PDR component around HD 34078. In order to avoid false detection of variations due to instrumental changes (e.g. spectral resolution) or to variations in stellar features blended with the H_2 line considered, we require that at least two lines from the same level display the same behavior. We then focus on those levels from which several lines with a high degree of significance and intermediate opacity values ($\tau_0 \simeq$ 1–5) are detected (e.g. $J = 9$, ($v = 1$, $J = 1, 2, 3$)). Occasionally, we observe apparent variations e.g. for the $v = 1$ lines at 1052.6 Å ($J = 1$) and 1056.8 Å ($J = 3$) for which a decrease in W by about 20% between epoch 1 and 2 is suggested by the data. However, we cannot find any H_2 level for which unambiguous evidence for a column density variation can be obtained. Often, the shape of the continuum adjacent to absorption lines is not stable (probably because of changes in the profile of underlying stellar absorption) which greatly complicates the comparison of spectra and the estimate of uncertainties on W or N variations. We thus conclude that the FUSE data exclude the existence of large variations in excited H_2 lines (larger than about 30%). Clearly, HST spectra would be very helpful to better constrain the temporal behavior of highly excited H_2 absorption thanks to both a higher resolution and *S/N* ratio.

5.4. HI

The Lyβ line offers an interesting opportunity to search for N(HI) variations. As already mentioned, the N(HI) value obtained from modelling the H_2–Lyβ blend is larger than the estimate drawn from IUE observations (Mc Lachlan & Nandy 1984). In Fig. 11 we show the spectral region used to determine N(HI) from the Lyβ–H_2 blend together with synthetic profiles computed with the 1979 and 2000 N(HI) values.

To assess whether the two determinations are really inconsistent, we have reanalysed the Lyα data. In the spectrum that we retrieved from the IUE database there is some weak residual flux at the bottom of the damped Lyα profile (while, given the spectral resolution, the profile should reach the zero level in the absence of scattered light). Correcting for this offset and fitting the Lyα profile again, we get a value – $\log(N(\mathrm{HI})) = 21.30$ – slightly larger than that given by Mc Lachlan & Nandy (1984): $\log(N(\mathrm{HI})) = 21.24$. This revised N(HI) remains significantly lower than the January 2000 value. Although it is difficult to reach a firm conclusion regarding the reality of a change in N(HI) because we could not compare the same feature from both epochs and because the Lyβ line is strongly blended with H_2 absorption, our analysis suggests that the HI column density towards HD 34078 has increased by 38% between 1979 and 2000 (this time interval corresponds to a transverse separation of 300 AU if the HI is assumed to lie at $d = 400$ pc). The corresponding average increase rate for N(HI) would be 1.8%/yr, which turns out to be comparable to the rate implied by CH observations (1.7%/yr; Rollinde et al. 2003).

On smaller scales, the ubiquitous structure in the atomic phase (Heiles 1997) should be apparent if our sensitivity to variations in the Lyβ profile is good enough (most of the HI is likely unassociated with HD 34078). Modelling of the profile indicates that the region near 1026.9 Å (rest wavelength), at

the red end of the trough, is best suited to search for N(HI) variation. At longer wavelengths, where larger variations would be expected, strong lines are present as well as OVIλ1031 variable absorption from the O star wind. We carefully compare the five profiles in this region (after adjusting the wavelength and flux scales as explained in Sect. 4.2 above) and find no evidence for any variation larger than 10% (the exact upper limit is difficult to define but we estimate that a 10% variation would unambiguously be seen; 10% is therefore equivalent to a 3σ limit).

5.5. Discussion

The main goal of our work is to study the AU scale structure in the spatial distribution of H_2 through the temporal behavior of its absorption lines. Concerning the bulk of molecular gas (i.e. $J = 0$ and 1 levels) which is believed to lie far from HD 34078, no profile variation is detected, which implies column density fluctuations lower than 5% over scales ranging from 5 to 50 AU. We conclude that translucent clouds display no "ubiquitous" small scale structure in molecular hydrogen such as that seen for H_2CO, OH or in the atomic phase through HI 21 cm absorption (Heiles 1997) or NaI optical lines. Our sampling remains limited, but since we observed five distinct positions, from 5 to 50 AU apart, one can reliably conclude that a line of sight with $N(H_2) \simeq 3 \times 10^{20}$ cm^{-2}, does not in general intersect clumps of this length scale with $N(H_2)$ larger than 1.5×10^{19} cm^{-2}.

The observed absence of ubiquitous $N(H_2)$ fluctuations in translucent clouds is an important result in that it tells us that uniform models can legitimately be used to describe chemical and physical processes within interstellar gas (which we did above in Sect. 4 !). Structure might be present at larger scales and it is noteworthy that direct CO emission imaging using millimeter wave interferometers can now probe structure at scales as small as 500 AU, i.e. barely one order of magnitude larger than those explored here. A few projects of this type are in progress; preliminary results indicate some velocity structure but modest column density variations (Falgarone, private communication).

CH observations have indicated a 20% increase of N(CH) over the last 12 years (Rollinde et al. 2003). Since CH and H_2 appear to be well correlated from one line of sight to another, one can search for any such trend in the FUSE data. The two extreme FUSE observations are separated by 2.7 yr and show no hint of such a variation. Assuming that the rate of increase is constant (about 1.7%/yr for N(CH); in fact the shape of this variation is not well constrained: cf Rollinde et al. 2003), an increase of $N(H_2)$ by 4.5% would be expected if a linear correlation still holds at small scales. This is just below what we can detect. Therefore, the present data do not allow us to check whether the long-term evolution of CH and H_2 is similar.

Regarding highly excited H_2, the time behavior of its absorption lines is related, in the frame of the model sketched in Sect. 4, to the stability of the gas flow in the shocked gas layer, at the interface of the stellar wind and the ambient medium in which HD 34078 is moving. If the latter is not homogeneous in the 1–100 AU scale range, this will induce line variations resulting from fluctuations of the amount of gas swept up by the bow shock and then compressed in the cylindrical layer around HD 34078. Variations due to instabilities in the interface could also occur, even if the ambient medium is homogeneous. The lack of pronounced variations indicates that the medium through which HD 34078 is moving is smooth and, further, that marked instabilities do not develop at the interface.

6. Summary and prospects

The analysis of five HD 34078 FUSE spectra taken between January 2000 and October 2002 leads to the following conclusions:

- The unexpectedly large amount of higly excited H_2 is attributed to the presence of molecular gas in a dense layer surrounding HD 34078 and excited by fluorescence. Detailed modelling of this region provides a very good fit to the excitation diagram, with few free parameters.
- The bulk of the molecular gas (H_2 ($J = 0$, 1), CH, CH^+, CO etc.) lies in a foreground translucent cloud, presumably unrelated to HD 34078. Physical conditions (temperature, density, etc.) are similar to those seen in diffuse molecular gas in general.
- The stability of damped H_2 absorption lines from $J = 0$, 1 and 2 levels indicate that H_2 molecules are smoothly distributed within the foreground translucent cloud with column density fluctuations lower than 5% over scales ranging from 5 to 50 AU.
- H_2 lines from highly excited levels also turn out to be stable. Again, this points towards a smooth distribution of H_2 molecules in the diffuse ambient medium through which HD 34078 is presently moving and indicates that no instability is developing in the shocked gas flow around HD 34078.

Let us conclude with a few prospects concerning the study of this very interesting line of sight. As discussed above, our analysis of small scale structure assumes that the translucent cloud lies far away in front of HD 34078 and thus heavily relies on a good understanding of the location of the gas responsible for the various absorptions observed. It is then important to find additional support for the two-component model proposed. We first plan to map the CO emission in the close environment of the HD 34078 line of sight. If our assumption is correct, there should be no relation between the morphology of the observed CO emission and the position of the O star or the direction of its motion (essentially northward). While comparing the radial velocity (and velocity dispersion) of the absorptions arising from each of the two main components, the limited FUSE resolution prevented us to reach definite conclusions. HST/STIS observations would be invaluable in this respect. Thanks to a higher resolution and *S/N*, HST spectra would also allow us to much better characterise both the kinematical and physical properties of the translucent and hot PDR components, through detection of H_2 lines from higher excitation levels (cf the study by Meyer et al. 2001) as well as from CI or CO. Finally, the Lyα profile would give an accurate N(HI) determination and then allow us to confirm the reality of the long-term N(HI) variation.

Acknowledgements. We thank J. Black and S. Federman for helpful remarks and the referee for several constructive comments which contributed to clarifying and strengthening the content of this paper. We also thank D. Meyer for providing the numerical values of the column densities of vibrationally excited H_2 towards HD37903. This work has been done using the profile fitting procedure OWENS developed by M. Lemoine and the FUSE French Team that we would like to thank for their help.

References

Abgrall, H., Roueff, E., Launay, F., Roncin, J. Y., & Subtil, J. L. 1993a, A&AS, 101, 273
Abgrall, H., Roueff, E., Launay, F., Roncin, J. Y., & Subtil, J. L. 1993b, A&AS, 101, 323
Allen, M. 1994, ApJ, 424, 754
Alves, J., Lada, C. J., & Lada, E. A. 2001, Nature, 409, 159
Crawford, D. L. 1975, PASP, 87, 481
Bohlin, R. C., Savage, D., & Drake, J. F. 1978, ApJ, 224, 132
Boissé, P., Rollinde, E., Le Petit, F., et al. 2001, in Gaseous Matter in Galaxies and Intergalactic Space, 17th IAP Astrophysics Colloquium, ed. R. Ferlet, et al., 41
Brown, A. G. A., Hartmann, D., & Burton, W. B. 1995, A&A, 300, 903
Draine, B. 1978, ApJS, 36, 595
Federman, S. R., Strom, C. J., Lambert, D. L., et al. 1994, ApJ, 424, 772
Federman, S. R., Cardelli, J. A., Lambert, D. L., et al. 1995, ApJ, 445, 325
Felenbok, P., & Roueff, E., 1996, ApJ, 465, L57
Fitzpartrick, E. L., & Massa, D. 1990, ApJS, 72, 163
Flower, D. R., & Pineau des Forêts, G. 1998, MNRAS, 297, 1182
Gredel, R., Pineau des Forêts, G., & Federman, S. 2002, A&A, 389, 993
Gry, C., Boulanger, F., Nehmé, C., et al. 2002, A&A, 391, 675
Heiles, C. 1997, ApJ, 481, 193
Herbig, G. H. 1958, PASP, 70, 468
Herbig, G. H. 1999, PASP, 111, 809
Lada, C. J., Alves, J., & Lada, E. A. 1999, ApJ, 512, 250
Le Bourlot, J., Pineau des Forêts, G., Roueff, E., & Flower, D. 1993, A&A, 267, 233
Lee, D.-H., Min, K.-W., Federman, S. R., et al. 2002, ApJ, 575, 239
Le Petit, F., Boissé, P., Roueff, E., Gry, C., & Le Brun, V. 2000, in IAU joint discussion, 11, 11
Le Petit, F., Boissé, P., Pineau des Forêts, G., et al. 2001, in Gaseous Matter in Galaxies and Intergalactic Space, 17th IAP Astrophysics Colloquium ed. R. Ferlet, et al., 45
Le Petit, F., Roueff, E., & Le Bourlot, J. 2002, A&A, 390, 369
Le Petit, F., Herbst, E., & Roueff, E. 2004, A&A, 417, 993
Liszt, H., & Lucas, R. 2000, A&A, 355, 333
Mc Lachlan, A., & Nandy, K. 1984, MNRAS, 207, 355
Mac Low, M., van Buren, D., Wood, D., & Churchwell, E. 1991, ApJ, 369, 395
Meyer, D. M., Lauroesch, J. T., Ulysses, J., Sofia, et al. 2001, ApJ, 553, L59
Moffat, A. F. J., Marchenko, S. V., Seggewiss, W., et al. 1998, A&A, 331, 949
Moore, E. M., & Marscher, A. P. 1995, ApJ, 452, 671
Moos, H. W., Cash, W. C., Cowie, L. L., et al. 2000, ApJ, 538, L1
Morton, D. C. 1975, ApJ, 197, 85
Morton, D. C. 2000, ApJS, 130, 403
Oka, T., Thorburn, J. A., McCall, B. J., et al. 2003, ApJ, 582, 823
Patriarchi, A., Morbidelli, L., Perinotto, M., & Barbaro, G. 2001, A&A, 372, 644
Rollinde, E., Boissé, P., Federman, S. R., & Pan, K. 2003, A&A, 401, 215
Rollinde, E. 2003, Ph.D. Thesis, University Paris XI
Sahnow, D. J., Moos, H. W., Ake, T. B., et al. 2000, ApJ, 538, L7
Snow, T. P. 1977, ApJ, 216, 724
Thoraval, S., Boissé, P., & Stark, R. 1996, A&A, 312, 973
Thoraval, S., Boissé, P., & Duvert, G. 1997, A&A, 319, 948
Thoraval, S., Boissé, P., & Stark, R. 1999, A&A, 351, 1051
van Buren, D., Mac Low, M.-M., Wood, D. O. S., & Churchwell, E. 1990, ApJ, 353, 570
van Buren, D., Noriega-Crespo, A., & Dgani, R. 1995, AJ, 110, 2914
Wright, E. L., & Morton, D. C. 1979, ApJ, 227, 483